Available online at www.sciencedirect.com
SCIENCE DIRECT
ELSEVIER
International Journal of Heat and Mass Transfer 49 (2006) 1375–1383
International Journal of HEAT and MASS TRANSFER
www.elsevier.com/locate/ijhmt

Coupled thermal and hydrodynamic models of flat micro heat pipes for the cooling of multiple electronic components

F. Lefèvre *, M. Lallemand

CETHIL, UMR 5008 CNRS-INSA-UCB, INSA, 20 av. A. Einstein, 69621 Villeurbanne Cedex, France

Received 23 May 2005; received in revised form 3 October 2005
Available online 22 November 2005

Abstract

An analytical solution for both the liquid and vapour flows inside a flat micro heat pipe (MHP) coupled to an analytical solution for the temperature inside the MHP wall is presented. The maximum heat transfer capability of a flat MHP, on which several heat sources and heat sinks are located, is calculated. The capillary structure inside the MHP is modeled by considering a porous medium, which allows to take into account capillary structures such as meshes or sintered powder wicks. The thermal model is able to calculate the part of heat flux transferred only by heat conduction in the MHP wall from the heat transferred by change of phase.
© 2005 Elsevier Ltd. All rights reserved.

Keywords: Micro heat pipe; Analytical model

1. Introduction

Substrates with high thermal conductivity are continually under development to meet the demand of increasing power density on electronic devices. Diamond is one of the materials having the greatest thermal conductivity, which ranges between 1000 and 2000 W m^{-1} K^{-1}, but its cost is very large. One way to obtain such or higher thermal conductivities at a lower cost is to micromachined two-phase micro heat pipes (MHPs) in a cheaper substrate of high conductivity material like copper, aluminum or silicon. A MHP is a cavity of small thickness, less than 1 mm, which is filled with a two-phase working fluid. Heat sources and heat sinks are located anywhere on the cavity with the other parts being thermally insulated. The heat sources can be electronic components or any system dissipating high heat fluxes and having to be maintained at a low or a constant temperature. The heat sinks can be any classical cooling devices. Vapour is generated at the heat source level and it condensates at the heat sink level. The liquid returns from the condenser to the evaporator through a capillary structure. For the cooling of electronic components, the more common working fluids are water, acetone, ethanol or methanol.

For both metallic and silicon MHPs, three types of capillary structure can be found in literature. The most simple MHPs have a single non-circular channel for both the liquid and the vapour phases [1–5]. For these MHPs, the liquid returns from the condenser to the evaporator by capillary flow in the sharp corners of the pipe. These types of MHP are generally placed in an array of parallel MHPs in order to increase the heat exchange area. Lots of works have been published for the thermal and hydrodynamic modeling of single MHPs or arrays of MHPs. Among them, Longtin et al. [6] have developed a 1D model based on the conservation equations and the Young–Laplace law to calculate the maximum heat transfer capability of a micro heat pipe of triangular cross section. Sartre et al. [7] have coupled the Longtin et al. [6] model to a thermal 2D conduction model, taking into account the high heat transfer in the contact area between the meniscus and the wall. More recently, Wang and Peterson [2] and Launay et al. [8] have improved the Longtin equations to model

* Corresponding author. Tel.: +33 4 7243 8251; fax: +33 4 7243 8811.
E-mail address: frederic.lefevre@insa-lyon.fr (F. Lefèvre).

0017-9310/$ - see front matter © 2005 Elsevier Ltd. All rights reserved.
doi:10.1016/j.ijheatmasstransfer.2005.10.001

Nomenclature

a, b, c	MHP dimensions, m
A_{m0}, A_{0n}, A_{mn}	Fourier coefficients of T^*
B, C	dimensionless lengths
Bi	Biot number
B_{m0}, B_{0n}, B_{mn}	Fourier coefficients of Φ
C_{m0}, C_{0n}, C_{mn}	Fourier coefficients of P
d	diameter of the mesh fibre, m
g	gravitational acceleration, $\mathrm{ms^{-2}}$
G	dimensionless parameter
h	heat transfer coefficient, $\mathrm{W\,m^{-2}\,K^{-1}}$
H	height, m
h_{lv}	latent heat of vaporisation, $\mathrm{J\,kg^{-1}}$
K	permeability, $\mathrm{m^2}$
N	mesh number
P	pressure, Pa
P^*	total pressure, Pa
Q	heat transfer rate, W
r	pore radius, m
T	temperature, K
T^*	dimensionless temperature
u	velocity along the x axis, $\mathrm{ms^{-1}}$
v	velocity along the y axis, $\mathrm{ms^{-1}}$
V	velocity, $\mathrm{ms^{-1}}$
w	distance between two fibres, m
x, y, z	coordinates, m
X, Y, Z	dimensionless coordinates

Greek symbols

$\phi\ (X, Y)$	dimensionless heat flux
η	ratio between the evaporator and condenser areas
φ	heat flux, $\mathrm{W\,m^{-2}}$
φ_0	imposed heat flux, $\mathrm{W\,m^{-2}}$
λ	thermal conductivity, $\mathrm{W\,m^{-1}\,K^{-1}}$
μ	dynamic viscosity, Pa s
ρ	density, $\mathrm{kg\,m^{-3}}$
σ	surface tension, $\mathrm{N\,m^{-1}}$
ξ	porosity

Subscripts

c	condenser
cap	capillary
eff	effective
e	evaporator
eq	equivalent
g	gravity
l	liquid
max	maximum
p	porous medium
s	solid
sat	saturation
v	vapour
w	wall

arrays of micro heat pipes made of several aluminum wires bonded between two aluminum sheets.

The second configuration deals with MHPs having a single vapour core and a one dimensional capillary structure such as parallel grooves [9,10]. As the capillary flow is 1D, 1D hydrodynamic models are often sufficient to calculate the performances of this type of MHP. Lefèvre et al. [11] developed a 1D hydrodynamic model based on the Longtin equations to calculate the maximum heat power capability of such a MHP. The comparison with the experimental results of Hopkins et al. [9] shows good agreement between the experimental and calculated performances.

An other configuration deals with MHPs having a single vapour core and a 2D capillary structure, such as metallic meshes [12] or crossed grooves [13,14]. A 2D capillary structure is well adapted to electronic cooling. Indeed, it allows the spreading of heat in two directions and thus several electronic components placed anywhere on the same MHP can be cooled. Huang and Liu [15] have presented a 2D hydrodynamic model for the liquid flow in a flat plate heat pipe. This model has been modified by Qin and Liu [16] to take into account an anisotropic capillary structure. Tan et al. [17] have developed a similar model using a point source approach to optimise the locations of several electronic components on flat heat pipes. Nevertheless, in all these models, the vapour flow inside the MHP is not taken into account, whereas, the pressure drop in the vapour phase can be important because of the thickness of the internal vapour space.

In the present work we present a 2D hydrodynamic model for both the liquid and the vapour flows coupled to a 3D thermal model, which allows to consider several electronic components and heat sinks on a flat plate heat pipe. If the thermal resistance of the wall is small, it is important to take into account the heat conduction inside the MHP wall. Indeed, if the distance between the heat source and the heat sink is small enough, one part of the heat is transferred by conduction through the MHP wall. Furthermore, due to heat diffusion in the wall, the areas of condensation and evaporation are larger than the area of the electronic components and the heat sinks. Taking into account the heat diffusion in the wall leads to larger evaporating and condensing areas, which occur in the mass conservation equation of the hydrodynamic model.

2. Governing equations and boundary conditions

The geometry of the two-phase MHP is shown in Fig. 1. It consists of a flat plate of $a \times b$ rectangular dimensions. The electronic components and the heat sinks can be located at different places on the MHP and have different heat powers. The rest of the surface is adiabatic. The wall

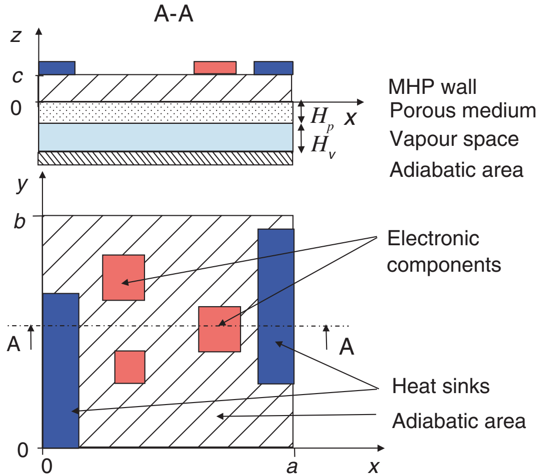

Fig. 1. Scheme of a two-phase MHP with heat sources and heat sinks.

of the MHP is made of a material of thermal conductivity λ_s and its height is equal to c. The capillary structure is modeled by considering a porous medium of permeability K, heat conductivity λ_p and height H_p. The liquid inside the porous medium has a dynamic viscosity μ_l, a heat conductivity λ_l and a density ρ_l. The equivalent conductivity of both the liquid and the porous medium is equal to λ_{eq}. The vapour space height is equal to H_v, and λ_v and μ_v are the vapour heat conductivity and dynamic viscosity, respectively. The thermal properties are supposed to be constant inside the MHP. They are calculated at the saturation temperature T_{sat}.

A 3D thermal model has been developed, assuming that, apart from the heat sources and the heat sinks, all the surfaces of the MHP are well insulated. This thermal model has been developed on the basis of a work published by Fen and Xu [18], which is about a one phase heat spreader in metal, dissipating heat only by conduction through the metal to a fin. In the present model, the heat supplied by the electronic components is transferred through the MHP wall to the porous medium where it causes the evaporation of the liquid. At the level of the heat sink, the vapour condensates and finally the heat is transferred by conduction through the wall to the heat sink. If the distance between the heat source and the heat sink is small enough, one part of the heat can be transferred by conduction through the MHP wall.

The steady-state heat conduction equation in three dimensions is solved in the MHP wall, assuming its thermal conductivity λ_s is constant. The boundary condition at $z = c$ is an imposed heat flux φ_0 at the electronic component area, an imposed heat flux equal to $-\eta \times \varphi_0$ at the heat sink area (η being the ratio between the heat sinks and the heat sources areas) and a heat flux equal to zero in the adiabatic area. A Fourier condition is taken into account at the junction between the MHP wall and the porous medium; the saturation temperature T_{sat} being the vapour temperature, which is supposed to be constant. The heat transfer coefficient h is calculated by considering the thermal conductance of the porous medium filled with liquid.

Let us introduce the non-dimensional coordinates X, Y and Z:

$$X = \frac{x}{a}; \quad Y = \frac{y}{b}; \quad Z = \frac{z}{c} \tag{1}$$

If $\Delta T = T - T_{sat}$ is the temperature difference between the local and the saturation temperatures, the 3D steady-state heat conduction equation can be written as

$$\frac{\partial^2 T^*}{\partial X^2} + \frac{1}{B^2}\frac{\partial^2 T^*}{\partial Y^2} + \frac{1}{C^2}\frac{\partial^2 T^*}{\partial Z^2} = 0 \tag{2}$$

with the dimensionless temperature defined as follows:

$$T^* = \frac{\lambda_s}{\varphi_0 c}\Delta T; \quad B = \frac{b}{a}; \quad C = \frac{c}{a} \tag{3}$$

The boundary conditions are written as

$$\left.\frac{\partial T^*}{\partial X}\right|_{X=0} = \left.\frac{\partial T^*}{\partial X}\right|_{X=1} = 0 \tag{4}$$

$$\left.\frac{\partial T^*}{\partial Y}\right|_{Y=0} = \left.\frac{\partial T^*}{\partial Y}\right|_{Y=1} = 0 \tag{5}$$

$$\left.\frac{\partial T^*}{\partial Z}\right|_{Z=0} = \frac{hc}{\lambda}T^* = BiT^* \tag{6}$$

$$\phi(X,Y) = \left.\frac{\partial T^*}{\partial Z}\right|_{Z=1} = \begin{cases} 1 & \text{in the evaporator area} \\ 0 & \text{in the adiabatic area} \\ -\eta & \text{in the condenser area} \end{cases} \tag{7}$$

where Bi is the Biot number and $\phi(X, Y)$ is the non-dimensional heat flux. Depending on the boundary conditions, the non-dimensional temperature T^* can be expanded in a form of an infinite Fourier series as

$$T^* = \sum_{m=1}^{\infty} A_{m0}(Z)\cos(m\pi X) + \sum_{n=1}^{\infty} A_{0n}(Z)\cos(n\pi Y) + \sum_{n=1}^{\infty}\sum_{m=1}^{\infty} A_{mn}(Z)\cos(m\pi X)\cos(n\pi Y) \tag{8}$$

The non-dimensional heat flux can be written using the following expression:

$$\phi(X,Y) = \sum_{m=1}^{\infty} B_{m0}\cos(m\pi X) + \sum_{n=1}^{\infty} B_{0n}\cos(n\pi Y) + \sum_{n=1}^{\infty}\sum_{m=1}^{\infty} B_{mn}\cos(m\pi X)\cos(n\pi Y) \tag{9}$$

The expressions of B_{m0}, B_{0n} and B_{mn} depend on the location of the heat sources and the heat sinks (Fig. 2). For a rectangular evaporator i of coordinates $[a_{e1}(i), a_{e2}(i), b_{e1}(i), b_{e2}(i)]$, the value of B_{m0}, B_{0n} and B_{mn} are equal to

$$B_{m0} = \frac{2}{m\pi b}\left\{\sin\left[\frac{m\pi a_{e2}(i)}{a}\right] - \sin\left[\frac{m\pi a_{e1}(i)}{a}\right]\right\} \times [b_{e2}(i) - b_{e1}(i)] \tag{10}$$

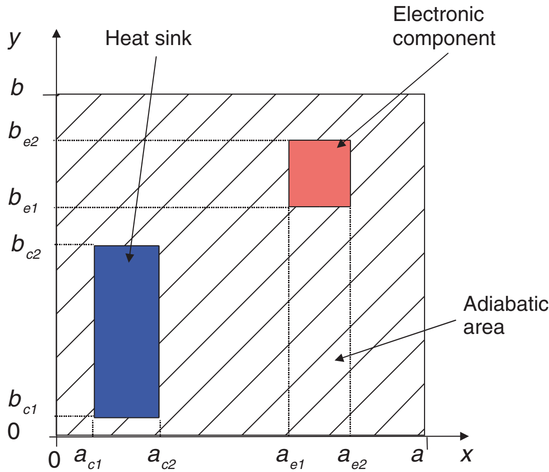

Fig. 2. Coordinates of heat sources and heat sinks.

$$B_{0n} = \frac{2}{n\pi a}\left\{\sin\left[\frac{n\pi b_{e2}(i)}{b}\right] - \sin\left[\frac{n\pi b_{e1}(i)}{b}\right]\right\} \times [a_{e2}(i) - a_{e1}(i)] \quad (11)$$

$$B_{mn} = \frac{4}{mn\pi^2}\left\{\sin\left[\frac{m\pi a_{e2}(i)}{a}\right] - \sin\left[\frac{m\pi a_{e1}(i)}{a}\right]\right\} \times \left\{\sin\left[\frac{n\pi b_{e2}(i)}{b}\right] - \sin\left[\frac{n\pi b_{e1}(i)}{b}\right]\right\} \quad (12)$$

For a rectangular condenser j of coordinates $[a_{c1}(j), a_{c2}(j), b_{c1}(j), b_{c2}(j)]$ the value of B_{m0}, B_{0n} and B_{mn} can be obtained by multiplying the previous expressions by $-\eta$. By substituting Eqs. (8) and (9) into Eqs. (2), (6) and (7), we obtain the following expressions for coefficients A_{m0}, A_{0n} and A_{mn}:

$$A_{m0}(Z) = \frac{B_{m0}[(m\pi C + Bi)\exp(m\pi CZ) + (m\pi C - Bi)\exp(-m\pi CZ)]}{m\pi C[(m\pi C + Bi)\exp(m\pi C) - (m\pi C - Bi)\exp(-m\pi C)]} \quad (13)$$

$$A_{0n}(Z) = \frac{B_{0n}\left[\left(\frac{n\pi C}{B} + Bi\right)\exp\left(\frac{n\pi CZ}{B}\right) + \left(\frac{n\pi C}{B} - Bi\right)\exp\left(-\frac{n\pi CZ}{B}\right)\right]}{n\pi C[(n\pi C + BBi)\exp\left(\frac{n\pi C}{B}\right) - (n\pi C - BBi)\exp\left(-\frac{n\pi C}{B}\right)]} \quad (14)$$

$$A_{mn}(Z) = \frac{B_{mn}[(G\pi C + Bi)\exp(G\pi CZ) + (G\pi C - Bi)\exp(-G\pi CZ)]}{G\pi C[(G\pi C + Bi)\exp(G\pi C) - (G\pi C - Bi)\exp(-G\pi C)]} \quad (15)$$

where

$$G = \sqrt{m^2 + \left(\frac{n}{B}\right)^2} \quad (16)$$

3. Hydrodynamic model

As the internal height of the MHP is small compared to its dimensions a and b, a 2D hydrodynamic model has been developed for both the liquid and the vapour flows. Through the permeability K of the medium, many capillary structures can be modeled such as rectangular grooves, crossed grooves, metallic meshes or sintered metal powder wicks. Nevertheless, it has to be noticed that for grooved wick structures, the thinning of the fluid film that occurs in evaporator sections would affect the resistance of the film. This is not taken into account in the thermal model in which the equivalent thermal conductivity of the porous medium is assumed to be constant. The hydrodynamic model is based on the Huang and Liu [15] model for a porous medium. It has been extended to take into account the vapour flow inside the MHP. The 2D hydrodynamic model permits the calculation of both the vapour and liquid velocities in the MHP. Knowing the capillary pressure, it is possible to calculate the maximum heat transfer capability of the MHP.

3.1. Hydrodynamic model for the liquid

The liquid velocity normal to the vapour–liquid interface (in the z direction) is assumed to be zero. The governing equations for the liquid flow can therefore be expressed by the Darcy's law:

$$u_l = -\frac{K}{\mu_l}\frac{\partial P_l}{\partial x} \quad (17)$$

$$v_l = -\frac{K}{\mu_l}\frac{\partial P_l}{\partial y} \quad (18)$$

P is the pressure, u and v are the velocities in the x and y directions, respectively, and the subscript l denotes the liquid. These equations assume that the permeabilities are the same in the x and y directions, but it is possible to consider an anisotropic wick of permeability K_x and K_y along the x and y directions as it is shown by Qin and Liu [16].

The mass balance for the liquid can be written by the following expression:

$$\frac{\partial u_l}{\partial x} + \frac{\partial v_l}{\partial y} = \frac{1}{h_{lv}\rho_l H_p}\varphi\bigg|_{z=0} \quad (19)$$

in which h_{lv} is the latent heat of vaporisation and φ the heat flux, which can be any function of x and y. In this case, φ is calculated in the thermal model at z equal to zero:

$$\varphi|_{z=0} = \varphi_0 Bi T^*|_{z=0} \quad (20)$$

Introducing Eqs. (17) and (18) into Eq. (19) leads to the following second order differential equation:

$$\frac{\partial^2 P_l}{\partial x^2} + \frac{\partial^2 P_l}{\partial y^2} = -\frac{\mu_l}{K h_{lv}\rho_l H_p}\varphi\bigg|_{z=0} = -\frac{\mu_l}{K h_{lv}\rho_l H_p}\varphi_0 Bi T^*\bigg|_{z=0} \quad (21)$$

As the velocities u_l and v_l are equal to zero on the (x, y) boundaries, the boundary conditions for the pressure are:

$$\frac{\partial P_l}{\partial x}\bigg|_{x=0} = \frac{\partial P_l}{\partial x}\bigg|_{x=a} = \frac{\partial P_l}{\partial y}\bigg|_{y=0} = \frac{\partial P_l}{\partial y}\bigg|_{y=b} = 0 \quad (22)$$

With those boundary conditions, the pressure can be expressed in Fourier's series:

$$P_{\rm l} = \frac{\mu_{\rm l}}{Kh_{\rm lv}\rho_{\rm l}H_{\rm p}}\left[\sum_{m=1}^{\infty} C_{m0}\cos(m\pi X) + \sum_{n=1}^{\infty} C_{0n}\cos(n\pi Y) + \sum_{n=1}^{\infty}\sum_{m=1}^{\infty} C_{mn}\cos(m\pi X)\cos(n\pi Y)\right] \quad (23)$$

By introducing Eqs. (8) and (23) into Eq. (21), and comparing the terms on both sides of these equations, the coefficients C_{m0}, C_{0n} and C_{mn} are determined as

$$C_{m0} = \varphi_0 Bi\left(\frac{a}{m\pi}\right)^2 A_{m0}(0) \quad (24)$$

$$C_{0n} = \varphi_0 Bi\left(\frac{b}{n\pi}\right)^2 A_{0n}(0) \quad (25)$$

$$C_{mn} = \varphi_0 Bi\frac{1}{\left(\frac{m\pi}{a}\right)^2 + \left(\frac{n\pi}{b}\right)^2} A_{mn}(0) \quad (26)$$

The velocities u and v can easily be deduced from Eqs. (17), (18) and (23). If the MHP is not in a horizontal position, it is possible to take into account the body forces acting in the pressure field:

$$P_{\rm l}^* = P_{\rm l} + \rho_{\rm l} g H_{\rm l}(x,y) \quad (27)$$

where g is the gravity field and $H_{\rm l}(x,y)$ is the liquid height at the coordinates x and y inside the MHP.

3.2. Hydrodynamic model for the vapour

For the vapour, a similar approach has been adopted to calculate the pressure and the velocity fields inside the MHP. Assuming that the vapour flow is laminar between two parallel plates, we obtain the following expressions for the velocity components [19]:

$$u_{\rm v} = -\frac{H_{\rm v}^2}{12\mu_{\rm v}}\frac{\partial P_{\rm v}}{\partial x} \quad (28)$$

$$v_{\rm v} = -\frac{H_{\rm v}^2}{12\mu_{\rm v}}\frac{\partial P_{\rm v}}{\partial y} \quad (29)$$

in which the subscript v denotes the vapour and $H_{\rm v}$ the vapour channel height. These equations assume the vapour flow to be incompressible, which supposes that the axial vapour velocity is small compared to the velocity of sound. For the common working temperatures, this assumption is verified, which is not the case at low temperatures when the MHP starts.

The mass balance for the vapour has for expression:

$$\frac{\partial u_{\rm v}}{\partial x} + \frac{\partial v_{\rm v}}{\partial y} = -\frac{1}{h_{\rm lv}\rho_{\rm v}H_{\rm v}}\varphi\bigg|_{z=0} \quad (30)$$

Introducing Eqs. (28) and (29) into Eq. (30) leads to the following differential equation:

$$\frac{\partial^2 P_{\rm v}}{\partial x^2} + \frac{\partial^2 P_{\rm v}}{\partial y^2} = \frac{12}{H_{\rm v}^3}\frac{\mu_{\rm v}}{h_{\rm lv}\rho_{\rm v}}\varphi\bigg|_{z=0} = \frac{12}{H_{\rm v}^3}\frac{\mu_{\rm v}}{h_{\rm lv}\rho_{\rm v}}\varphi_0 BiT^*\bigg|_{z=0} \quad (31)$$

Assuming that the vapour velocities are equal to zero on the (x,y) boundaries leads to the following boundary conditions for the pressure:

$$\frac{\partial P_{\rm v}}{\partial x}\bigg|_{x=0} = \frac{\partial P_{\rm v}}{\partial x}\bigg|_{x=a} = \frac{\partial P_{\rm v}}{\partial y}\bigg|_{y=0} = \frac{\partial P_{\rm v}}{\partial y}\bigg|_{y=b} \quad (32)$$

from which, the pressure can be expressed in Fourier's series:

$$P_{\rm v} = -\frac{12}{H_{\rm v}^3}\frac{\mu_{\rm v}}{h_{\rm lv}\rho_{\rm v}}\left[\sum_{m=1}^{\infty} C_{m0}\cos(m\pi X) + \sum_{n=1}^{\infty} C_{0n}\cos(n\pi Y) + \sum_{n=1}^{\infty}\sum_{m=1}^{\infty} C_{mn}\cos(m\pi X)\cos(n\pi Y)\right] \quad (33)$$

where coefficients C_{m0}, C_{0n} and C_{mn} are given by Eqs. (24)–(26).

3.3. Maximum heat transfer capability of the MHP

The maximum heat transfer capability of the MHP is obtained when the following expression is verified:

$$\Delta P_{\rm cap} = \Delta P_{\rm l} + \Delta P_{\rm v} + \Delta P_{\rm g} \quad (34)$$

where the subscript g is related to gravitational forces and $\Delta P_{\rm cap}$ is the capillary pressure inside the MHP.

The capillary pressure can be calculated using the following classical expression, which results from the Young–Laplace law:

$$\Delta P_{\rm cap} = \frac{2\sigma}{r_{\rm eff}} \quad (35)$$

in which $r_{\rm eff}$ is the effective pore radius and σ is the surface tension of the fluid.

4. Validation with open literature data

In this section, we describe the comparison between the model and experimental results presented by Khandekar et al. [12]. The MHP under investigation is presented in Fig. 3. The heat pipe size is $40 \times 40\ \rm mm^2$, the condenser area is $15 \times 40\ \rm mm^2$ and the evaporator area is $10 \times 40\ \rm mm^2$. The total internal MHP thickness, including both the vapour space and the capillary structure is equal to 370 μm and the thickness of the wall under the sources is equal to 265 μm. The MHP is filled with water. The capillary structure is made of 2 or 3 CuSn 325 mesh screen layers. These two configurations have been tested in a vertical position with the evaporator below the condenser. As the wall thickness c is very small compared to dimensions a and b and as the heat sinks and the heat sources are not close, the heat conduction in the wall is negligible compared to the heat transfer by phase change in the heat pipe. Furthermore, the temperature measurements are not provided in the experimental paper. Khandekar et al. [12] present only the maximum heat flux versus the saturation

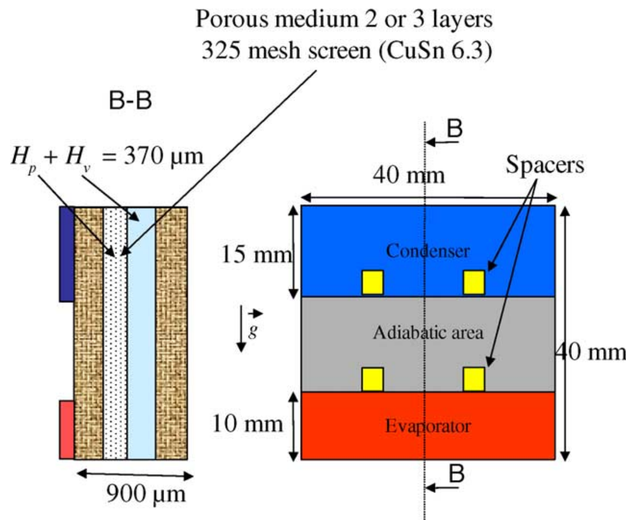

Fig. 3. Experimental MHP tested by Khandekar et al. [12].

temperature. Thus, these results do not allow the thermal model validation.

It is necessary to evaluate the porous medium properties to solve the thermal and hydrodynamic models. Porosity, permeability and effective radius are important parameters of the hydrodynamic model. The equivalent heat conductivity of the porous medium filled with liquid is used to calculate the heat conductance between the vapour and the junction of the MHP wall and the porous medium using relations given by Faghri [20].

For a mesh screen, the following expression permits the calculation of the permeability K:

$$K = \frac{d^2\xi^3}{122(1-\xi)^2} \tag{36}$$

in which d is the diameter of the mesh fibre and ξ its porosity. An evaluation of ξ is given by

$$\xi = 1 - \frac{1.05\pi Nd}{4} \tag{37}$$

where N is the mesh number, which depends on d and the distance between two fibres w:

$$N = \frac{1}{d+w} \tag{38}$$

For the considered porous medium, the fibre diameter is equal to 35 µm and w is equal to 42 µm. These geometrical properties lead to a permeability K equal to 1.8×10^{-11} m^2. The thickness of each mesh screen layer is equal to 70 µm.

An experimental value of 33 µm has been given by Faghri [20] for the effective pore radius of a 325 mesh screen in contact with water. The following expression, which depends on the thermal conductivity of both the liquid and the solid, permits the calculation of the equivalent thermal conductivity λ_{eq} [20]:

$$\lambda_{eq} = \frac{\lambda_l[(\lambda_l + \lambda_p) - (1-\xi)(\lambda_l - \lambda_p)]}{(\lambda_l + \lambda_p) + (1-\xi)(\lambda_l - \lambda_p)} \tag{39}$$

For this mesh screen the equivalent thermal conductivity is equal to about 1.3 W m^{-1} K^{-1} and the resulting conductance h is equal to

$$h = \frac{\lambda_{eq}}{H_p} \tag{40}$$

The comparison between the model and experimental data is shown in Fig. 4. Bold and dotted lines represent the model results and points the experimental data of Khandekar et al. [12] for two different MHPs. The first one has two mesh screen layers, which corresponds to a thickness equal to 140 µm and the second one has three mesh screen layers, which corresponds to a thickness equal to 210 µm.

As we can see in Fig. 4, the maximum heat power capability calculated by the model is about 10 W higher than the experimental value, which represents between 30% and 50% over prediction. Nevertheless, the variation of maximum heat transport capability with the saturation temperature is the same in both cases. In fact, in the experimental configuration, four deflection preventing spacers of size 3×3 mm^2 (Fig. 3) are machined to the housing frame. These spacers are not taken into account in the model despite the fact that they produce an important pressure drop in both the liquid and vapour spaces. Furthermore, a perfect bonding of the mesh to the frame has been considered in the model, which is probably not the case in the experimental MHP. The maximum heat power capability of the MHP increases with the increase of T_{sat}. This is due to a lower pressure drop for the liquid and the vapour because the viscosity of the fluid decreases with an increase in T_{sat}.

Fig. 4 shows that the performances are better for the porous medium having two-layers than for the three-layered case. This is due to the pressure drop in the vapour space which becomes high when H_v decreases. For example, at a saturation temperature equal to 50 °C, the pressure drop is equal to 3100 Pa in the vapour phase,

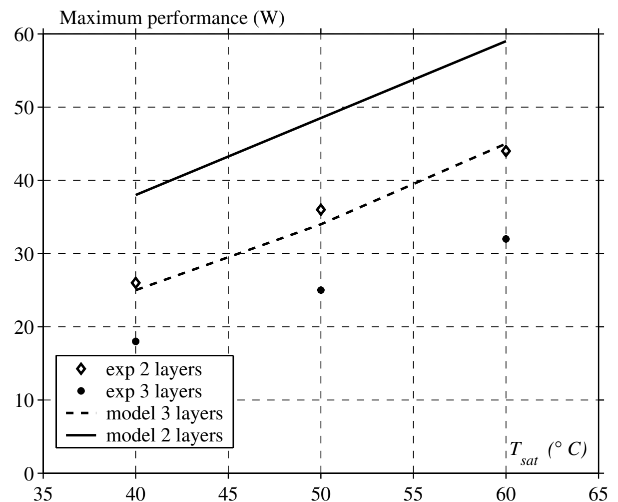

Fig. 4. Comparison between the model and experimental results [12].

whereas it is equal to 1000 Pa in the liquid phase for the MHP having three mesh screen layers. This example shows that the vapour pressure drop is important for a flat MHP.

5. Flow and isotherm patterns for several heat sinks and electronic components

In this last part, we present some simulations obtained with a MHP similar to the MHP tested by Kandhekar et al. [12], but having three electronic components (E_1, E_2 and E_3) and two heat sinks (C_1 and C_2) as shown in Fig. 1. It is assumed that the same heat flux φ_0 is imposed to the three electronic components. For both the heat sinks the heat flux is equal to $-\eta\varphi_0$. The capillary structure is made of two layers of CuSn 325 mesh screen. For the simulations, the saturation temperature is equal to 50 °C corresponding to a saturation pressure equal to 12,335 Pa. The MHP is supposed to be in horizontal position.

Figs. 5 and 6 present the isobars inside the MHP, for the vapour and the liquid, respectively. The rectangles in bold lines correspond to the electronic components location and the rectangles in dotted lines correspond to the heat sinks location. The vapour pressure is maximum under the electronic component E_1, which has the maximum heat transfer rate and thus, where the vapour generation is maximum. The vapour pressure, which is minimum under the heat sink C_1, is equal to the saturation pressure. The capillary structure is supposed to be entirely filled in the condenser where the vapour pressure is minimum. Thus, the meniscus radius between the liquid and the capillary structure is infinite and the liquid pressure is equal to the vapour pressure due to the Young–Laplace law. The minimum liquid pressure is located under the electronic component E_1, where the heat transfer rate is maximum.

As we can see, the pressure drop is about $\Delta P_l = 2600$ Pa in the liquid and $\Delta P_v = 1500$ Pa in the vapour corresponding to a maximum capillary pressure $\Delta P_{cap} = 4100$ Pa. The maximum capillary pressure, that depends on both the effective pore radius of the mesh screen and the fluid surface tension, is calculated with Eq. (35). Eq. (34) is satisfied when the maximum heat transfer rate Q_{max} is equal to 76 W, which corresponds to a heat flux equal to 35 W cm^{-2}. The electronic components E_1, E_2 and E_3 have a heat transfer rate equal to 50.2, 17.1 and 8.7 W, respectively. In this configuration, as the electronic component E_1 is very close to the heat sink C_1, about 13 W are dissipated only by heat conduction in the MHP wall though the MHP wall is very thin. This example shows that it is important to take into account the conduction through the wall to calculate the maximum heat transport capability of the MHP. Without heat conduction in the wall, the maximum heat transport capability of the MHP would have been 20% under predicted.

Figs. 7 and 8 show the vapour and liquid velocity field inside the MHP, respectively. The maximum velocities are about 31 ms^{-1} for the vapour and 4×10^{-3} ms^{-1} for the liquid. These maximum values of the liquid and vapour

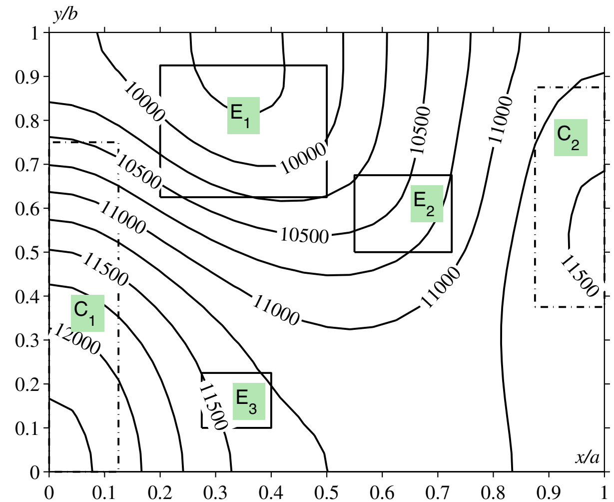

Fig. 6. Liquid isobars (Pa) ($T_{sat} = 50$ °C; $Q_{max} = 76$ W).

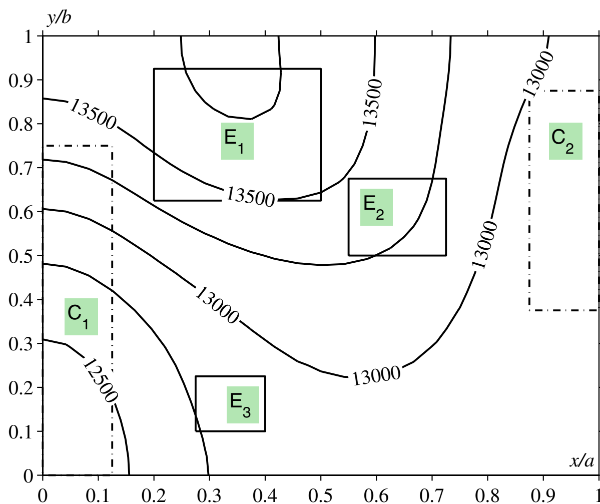

Fig. 5. Vapour isobars (Pa) ($T_{sat} = 50$ °C; $Q_{max} = 76$ W).

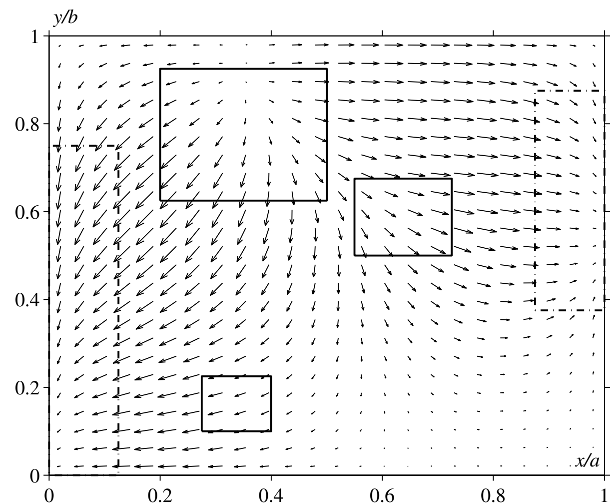

Fig. 7. Vapour velocities ($T_{sat} = 50$ °C; $Q_{max} = 76$ W; $V_{max} = 30.9$ ms^{-1}).

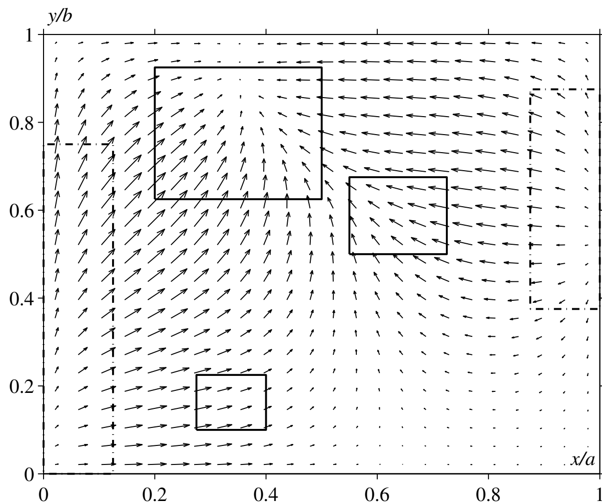

Fig. 8. Liquid velocities ($T_{sat} = 50$ °C; $Q_{max} = 76$ W; $V_{max} = 0.0043$ ms^{-1}).

phases are located between the evaporator E_1 and the condenser C_1, where the distance from a heat source to a heat sink is the lowest. The maximum Reynolds number is equal to 112 in the vapour phase, which corresponds to a laminar flow as it is assumed in the model. The characteristic dimension in the Reynolds number is equal to two times the height of the vapour space. These figures show the interest of using a capillary structure in two directions for cooling multiple electronic components. Indeed, as the liquid flow is 2D, the electronic components and the heat sinks can be located anywhere on the MHP in contrary to a 1D capillary structure where heat sources and heat sinks have to be located along the direction of the liquid flow.

In Fig. 9, the temperature difference between the wall temperature T_w at $z = c$ and the saturation temperature T_{sat} is shown for a heat flux equal to 35 W cm^{-2}. It is assumed that the saturation temperature is constant in

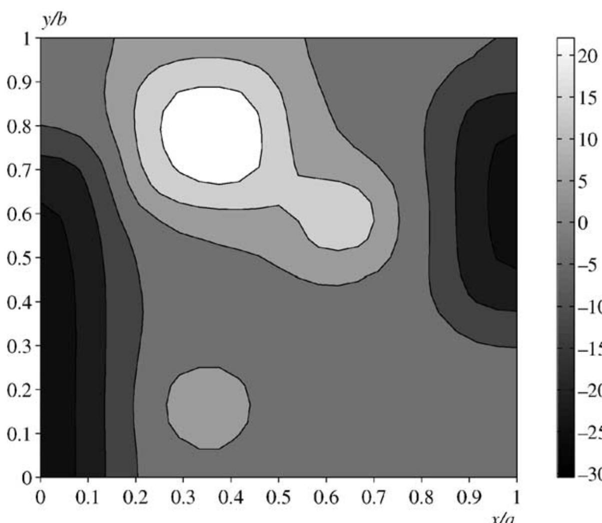

Fig. 9. Temperature difference ($T_w - T_{sat}$) (K) at $z = c$ for the MHP ($T_{sat} = 50$ °C; $Q_{max} = 76$ W).

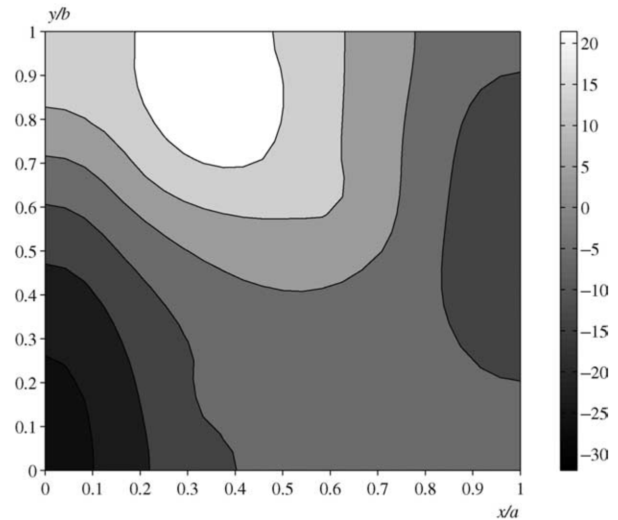

Fig. 10. Temperature difference ($T_w - T_{sat}$) (K) at $z = c$ for a full plate of thickness 635 μm and $\lambda = 1040$ W m^{-1} K^{-1} ($T_{sat} = 50$ °C; $Q_{max} = 76$ W).

the MHP. The maximum temperature difference, ΔT_{max} is about 50 K between the electronic component E_1 and the condenser C_1 or C_2. This high value is due to the low value of the porous wick equivalent thermal conductivity. A metallic sintered powder wick would have given better thermal performances. It has to be noticed that the liquid viscosity is evaluated at the saturation temperature. With such a temperature difference, the liquid viscosity is over estimated at the level of the condenser and under estimated at the level of the electronic component. This is a limitation of the model, in which it is assumed that the thermal properties are constant inside the MHP. Nevertheless, in the case of a full copper plate of same thickness than this MHP, the temperature difference raises to 140 K between the colder and the warmer point of the plate. With a full plate, a thermal conductivity of 1040 W m^{-1} K^{-1} would be necessary to obtain the same maximum temperature difference than that obtained with the MHP as it is shown in Fig. 10. Furthermore, even with such a thermal conductivity, the temperature field is not so homogeneous with a full plate than with a MHP.

6. Conclusion

A hydrodynamic 2D model for both the liquid and the vapour phases inside a MHP coupled to a 3D thermal model of heat conduction inside the MHP wall has been presented. The maximum heat transport capability of a MHP on which several electronic components and heat sinks are located can be predicted. The capillary structure is modeled by considering a porous medium. Through the permeability and the equivalent thermal conductivity of the porous medium, lots of capillary structures can be modeled. The comparison between the model and experimental data shows a good agreement between the calculated and the experimental maximum performances. The results show that it is important to model the pressure drop

inside the vapour phase in a flat plate MHP. This model allows the calculation of the part of the heat flux, which is dissipated only by heat conduction through the wall. The heat conduction through the MHP wall can modify the maximum performance of a MHP if the wall resistance is small enough.

References

[1] Y.X. Wang, H.B. Ma, G.P. Peterson, Investigation of the temperature distribution on radiator fins with micro heat pipes, J. Thermophys. Heat Transfer 15 (2001) 42–49.

[2] Y.X. Wang, G.P. Peterson, Analysis of wire-bonded micro heat pipe arrays, J. Thermophys. Heat Transfer 16 (2002) 346–355.

[3] S.H. Moon, G. Hwang, S.K. Ko, Y.T. Kim, Experimental study on the thermal performance of micro-heat pipe with cross-section of polygon, Microelectron. Reliab. 44 (2004) 315–321.

[4] S.W. Kang, D. Huang, Fabrication of star grooves and rhombus grooves micro heat pipe, J. Micromech. Micromeng. 12 (2002) 525–531.

[5] M. Le Berre, S. Launay, V. Sartre, M. Lallemand, Fabrication and experimental investigation of silicon micro heat pipes for cooling electronics, J. Micromech. Microeng. 13 (2003) 436–441.

[6] J.P. Longtin, B. Badran, F.M. Gerner, A one dimensional model of micro heat pipe during steady-state operation, J. Heat Transfer 116 (1994) 709–715.

[7] V. Sartre, M.C. Zaghdoudi, M. Lallemand, Effect of interfacial phenomena on evaporative heat transfer in micro heat pipes, Int. J. Therm. Sci. 39 (2000) 498–504.

[8] S. Launay, V. Sartre, M. Mantelli, K. De Paiva, M. Lallemand, Investigation of a wire plate micro heat pipe array, Int. J. Therm. Sci. 43 (2004) 499–507.

[9] R. Hopkins, A. Faghri, D. Khrustalev, Flat miniature heat pipes with micro capillary grooves, J. Heat Transfer 121 (1999) 102–109.

[10] L. Lin, R. Ponnappan, J. Leland, High performance miniature heat pipe, Int. J. Heat Mass Transfer 45 (2002) 3131–3142.

[11] F. Lefèvre, R. Revellin, M. Lallemand, Theoretical analysis of two-phase heat spreaders with different cross-section micro grooves, in: 7th Int. Heat Pipe Symposium, Jeju, Korea, October 12–16, 2003, pp. 97–102.

[12] S. Khandekar, M. Groll, V. Luckchoura, W. Findl, J. Zhuang, Micro heat pipes for stacked 3D microelectronic modules, in: Proc. of Interpack 2003—35109, 2003, 7p.

[13] D.A. Benson, R.T. Mitchell, M.R. Tuck, D.R. Adkins, D.W. Palmer, Micromachined heat pipes in silicon MCM substrates, in: IEEE Multi Chip Module Conference, Santa Clara, CA, 1996, pp. 127–129.

[14] D.A. Benson, R.T. Mitchell, M.R. Tuck, D.W. Palmer, G.P. Peterson, Ultrahighcapacity micromachined heat spreaders, Microscale Thermophys. Eng. 2 (1998) 21–30.

[15] X.Y. Huang, C.Y. Liu, The pressure and velocity fields in the wick structure of a localized heated flat plate heat pipe, Int. J. Heat Mass Transfer 39 (6) (1996) 1325–1330.

[16] W. Qin, C.Y. Liu, Liquid flow in the anisotropic wick structure of a flat plate heat pipe under block-heating condition, Appl. Therm. Eng. 17 (4) (1997) 339–349.

[17] B.K. Tan, X.Y. Huang, T.N. Wong, K.T. Ooi, A study of multiple heat sources on a flat plate heat pipe using a point source approach, Int. J. Heat Mass Transfer 43 (2000) 3755–3764.

[18] T.Q. Fen, J.L. Xu, An analytical solution of thermal resistance of cubic heat spreaders for electronic cooling, Appl. Therm. Eng. 24 (2004) 323–337.

[19] A. Bejan, Heat Transfer, Wiley, 1993.

[20] A. Faghri, Heat Pipe Science and Technology, Taylor and Francis, 1994.